Research Article Vol. 4, No. 5 / May 2017 / Optica 532

Ultra-low-loss Ta_2O_5-core/SiO_2-clad planar waveguides on Si substrates

Michael Belt,*,† Michael L. Davenport,† John E. Bowers, and Daniel J. Blumenthal

Electrical and Computer Engineering Department, University of California Santa Barbara, California 93106, USA
**Corresponding author: michaelbelt@ece.ucsb.edu*

Received 26 January 2017; revised 7 March 2017; accepted 16 March 2017 (Doc. ID 285717); published 9 May 2017

An increasing number of systems and applications depend on photonics for transmission and signal processing. This includes data centers, communications systems, environmental sensing, radar, lidar, and microwave signal generation. Such systems increasingly rely on monolithic integration of traditionally bulk optical components onto the chip scale to significantly reduce power and cost while simultaneously maintaining the requisite performance specifications at high production volumes. A critical aspect to meeting these challenges is the loss of the waveguide on the integrated optic platform, along with the capability of designing a wide range of passive and active optical elements while providing compatibility with low-cost, highly manufacturable processes, such as those found in CMOS. In this article, we report the demonstration of a record low propagation loss of 3 ± 1 dB/m across the entire telecommunications C-band for a CMOS-compatible Ta_2O_5-core/SiO_2-clad planar waveguide. The waveguide design, fabrication process, and optical frequency domain reflectometry characterization of the waveguide propagation loss and group index are described in detail. The losses and dispersion properties of this platform enable the integration of a wide variety of linear and nonlinear optical components on-chip, as well as integration with active rare-earth components for lasers and amplifiers and additionally silicon photonic integrated devices. This opens up new integration possibilities within the data communications, microwave photonics, high bandwidth electrical RF systems, sensing, and optical signal processing applications and research communities.

OCIS codes: (130.0130) Integrated optics; (230.7390) Waveguides, planar.

https://doi.org/10.1364/OPTICA.4.000532

1. INTRODUCTION

Ultra-low-loss Si_3N_4-core/SiO_2-clad planar waveguides (ULLWs) on silicon provide the basis of an integration platform allowing for a broad variety of exceptional active and passive photonics components, such as on-chip erbium-doped lasers [1], ultra-high-Q resonators [2], sidewall Bragg grating filters [3], and arrayed waveguide grating routers [4]. Such a platform is able to take advantage of the high index contrast between silica and silicon nitride to create waveguides that possess sub-millimeter bend radii and sub-dB/cm losses simultaneously. These characteristics enable applications previously supported only by fiber-based components to now be realized with a photonic integrated circuit (PIC) at a lower cost point and a smaller packaging footprint. Example applications include tunable optical true time delays for broadband phased array antennas [5–7], optical gyroscope rotational velocity sensors [8], and programmable dispersion compensating lattice filters [9].

However, the Si_3N_4-core-based platform possesses certain limitations that can be addressed through the substitution of Ta_2O_5 as a core material, as described in this work. For example, nonlinear optical processes on photonic chips can be used to generate and process signals all-optically with speeds far superior to electronics. For the best performance, such nonlinear processes generally require high mode confinement and dispersion engineering for phase matching [10,11]. Due to its high tensile film stress, depositing thick (>300 nm) layers of Si_3N_4 without cracking has historically proven to be a considerable fabrication challenge [10]. Furthermore, optical absorption in the 1.52 μm wavelength region due to nitrogen–hydrogen (N–H) bond resonances (hydrogen being an undesired impurity incorporated into the Si_3N_4 and SiO_2 films during fabrication) creates a "floor" on the lowest achievable optical loss within the C-band [12].

Tantalum pentoxide (Ta_2O_5) is a CMOS-compatible material [13,14] that presents the opportunity to address both the requirements for nonlinear interactions and the fundamental loss limitations of Si_3N_4 as a waveguide core material, while at the same time preserving a high index contrast that allows for small bend radii (the refractive index of Ta_2O_5 at 1550 nm is roughly the same as Si_3N_4, 2.05). Investigation of the nonlinear refractive index of Ta_2O_5 has shown that it has an order of magnitude higher value than that of silica (7.2×10^{-19} m^2/W for Ta_2O_5 [15] versus 2.2×10^{-20} m^2/W for SiO_2 [15]) and is greater than that of Si_3N_4 (2.4×10^{-19} m^2/W [16]), which allows for a shorter length of interaction and thus a reduced device footprint when

compared to both fiber and Si_3N_4-core based waveguides for achieving nonlinear applications such as optical switching. Due to the material's extremely large bandgap value (3.8 eV), two-photon absorption (TPA) and TPA-induced free-carrier absorption are of little to no concern when operating Ta_2O_5-based devices at high powers [17–19]. These important material parameters when considering waveguide design optimizations are summarized below in Table 1.

Furthermore, the broadband transparent nature of the material means that it is suitable for wavelengths spanning the ultraviolet to the long-wavelength infrared (300–8000 nm) [20]. Finally, due to the low value of film stress of Ta_2O_5 when compared to a Si_3N_4-core-based alternative (100 MPa for Ta_2O_5 versus 800 MPa for stoichiometric LPCVD Si_3O_4), fabricating thick, high mode confinement waveguides will be less of a fabrication challenge [21]. As well as the aforementioned benefits concerning nonlinear signal generation and processing, such a high confinement factor waveguide design would be advantageous in the development of active devices that leverage rare-earth ion dopants [22,23].

Attempts to date at reducing the loss of Ta_2O_5-core-based waveguides have focused on the core deposition and subsequent anneal steps of the fabrication process [24,25]. In [24], the authors employed a sputter deposition technique for the core region of their Ta_2O_5-core/SiO_2-clad waveguides, with an O_2 atmosphere anneal protocol immediately following. Their 400 nm thick waveguides were processed into ring resonator structures that showed a propagation loss of 1.5 dB/cm at wavelengths near 1550 nm. In [25], the authors incorporated a mixture of SiO_2 and Ta_2O_5 within the core region of their SiO_2-clad waveguide structures. Such a mixture allowed for a much higher maximum anneal temperature before the crystallization of the Ta_2O_5 than previously possible (1100°C versus 650°C) [26]. The resulting propagation loss was measured by applying the cutback method in waveguides with lengths between 2.7 and 23.9 cm. The 1.5 μm thick core waveguides displayed a loss of 6 dB/m at a wavelength of 1550 nm. Both of these loss values are most likely dominated by the large degree of waveguide sidewall scattering incurred during their reactive ion-based etching process.

In this paper, we report on record low propagation losses for Ta_2O_5-core/SiO_2-clad planar waveguides across the entire C-band over the lengths of complete spiral delays. Our structures demonstrate loss that is both lower than the state of the art for a Ta_2O_5-core waveguide [25] and that demonstrated by an Si_3N_4-core waveguide of an equivalent geometry [27]. We achieve these losses with refined core deposition and anneal processes, as well as through an optimized waveguide geometry and the resulting required etching protocol. We begin with an overview of the waveguide design and fabrication process. We then show optical backscattering reflectometry (OBR) characterization results from spiral waveguide delays. The group index and propagation loss of the waveguide structures are then reported.

Table 1. Material Parameters for Ta_2O_5, Si_3N_4, and SiO_2

	Parameter		
Material	Refractive Index (n) [$\lambda = 1550$ mn]	Nonlinear Refractive Index (n_2) [m^2/W]	Experimental Bandgap (E_g) [eV]
Ta_2O_5	2.05	7.2×10^{-19}	4.4
Si_3N_4	2.05	2.4×10^{-19}	5.3
SiO_2	1.44	2.2×10^{-20}	9

2. WAVEGUIDE DESIGN

The cross-sectional geometry and material stack for our waveguides follow the loss reduction and photonic integration approach reported in [27] and [28]. With Si_3N_4 and Ta_2O_5 having roughly equivalent optical indexes of refraction, the majority of waveguide design rules for Si_3N_4 core structures will also apply to waveguides featuring a Ta_2O_5 core. In general, when designing a waveguide cross section to minimize loss, there is an inherent compromise between optical confinement and core/cladding interfacial scattering loss. This trade-off manifests itself as an optimization between the lowest possible waveguide bend radius (as a practical matter, taking into account the given available on-chip PIC real estate) and the largest reduction in interfacial scattering loss contributions. When taking into account nonlinear applications, a high degree of optical confinement within the waveguide core is desirable, but this design parameter comes at the expense of an acute sensitivity to waveguide core sidewall scattering.

For planar waveguides, the roughness value at the waveguide sidewall due to optimized dry etching is typically an order of magnitude larger than that of the roughness value for the deposited top/bottom interfaces (1–10 nm versus <1 nm on average). This implies that the optimum lowest-loss single-mode core geometry for a given bend radius has the highest single-mode aspect ratio (width:thickness). Here, we choose a 90 nm Ta_2O_5 core thickness, with a width of 2.8 μm (the widest possible single-mode core width for the given core thickness). This high aspect ratio design (width:thickness > 10:1) ensures the waveguide will support only a single spatial mode in the C-band, while at the same time allowing tight (<1 mm, with no additional loss penalty) bends. Figure 1(a) gives a schematic representation of the cross section of the waveguide, while Fig. 1(b) gives shows the simulated (FIMMWAVE by Photon Design) transverse electric (TE) -polarized optical mode profile for the 1590 nm wavelength.

The transverse magnetic (TM) -polarized mode for such a geometry will have a lower confinement factor within the waveguide core (larger modal cross-sectional area) and thus a larger critical bend radius. The critical bend radius is defined as the

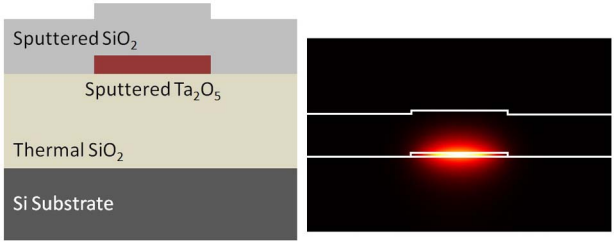

Fig. 1. (a) Cross-sectional geometry of the final Ta_2O_5-core/SiO_2-clad waveguide. The thermal SiO_2 lower cladding, Ta_2O_5 core, and sputtered SiO_2 upper claddings layers are 15 μm, 90 nm, and 1.1 μm thick, respectively. The width of the Ta_2O_5 core is 2.8 μm. (b) Simulated optical mode profile of the fundamental TE waveguide mode at the 1.55 μm wavelength. The calculated modal intensity diameters ($1/e^2$) are 2.7 μm in the horizontal by 1.1 μm in the vertical. These dimensions were confirmed experimentally through facet imaging utilizing an infrared camera. The calculated core confinement factor (Γ) is 0.15 and the effective index (n_{eff}) is 1.474.

radius at which the total propagation loss is dominated by the contribution from bend loss, rather than from the material or interfacial scattering losses. As a result of this bend limitation, combined with the maximum available field size of our lithography system, we consider in this work only TE-polarized light for waveguide design and loss measurements.

We designed the thickness of the upper and lower SiO_2 claddings as 1.1 and 15 μm, respectively. A thicker upper cladding layer would, in principle, result in a lower propagation loss, but in practice, even 2 μm thick sputter-deposited layers show a drastic decrease in film quality due to the incorporation of additional deleterious scattering centers. The 15 μm lower SiO_2 cladding ensures that the design is unaffected by leakage loss from the Si substrate.

3. DEVICE FABRICATION AND PROPAGATION LOSS CHARACTERIZATION

To test the optical loss of these waveguides, we designed and fabricated 10 m long Archimedean spiral delays with an innermost minimum bend radius of 2 mm and 0.7 m long spiral delays consisting of Bézier curves having a minimum bend radius of 760 μm and a central loop mirror structure. Figures 2(a) and 2(b) below give a schematic representation of both structures.

A. Waveguide Fabrication

Figures 3(a)–3(d) gives a graphical representation of the entirety of the Ta_2O_5 waveguide fabrication process.

Waveguide fabrication begins with a 1 mm thick, 100 mm diameter silicon substrate upon which 15 μm of silica is thermally grown by wet oxidation for the lower cladding. Next, 90 nm of Ta_2O_5 is deposited by sputter deposition. This 90 nm layer is then patterned using a photoresist mask by 248 nm stepper lithography and an optimized $CH_3/CF_4/O_2$ inductively coupled plasma etch. The etching chamber had $CH_3/CF_4/O_2$ gas flows of 35/5/10 cm^3/min, a pressure of 0.5 Pa, an RF source power of 500 W, and an RF bias of 50 W. This etching chamber is regularly used to etch various other materials (including Si, GaN, and InP) as part of our shared fabrication space, so if catastrophic contamination were to occur it would manifest during our loss measurements. Figures 4(a)–4(c) show atomic force microscopy (AFM) measurements of the waveguide core top and sidewalls

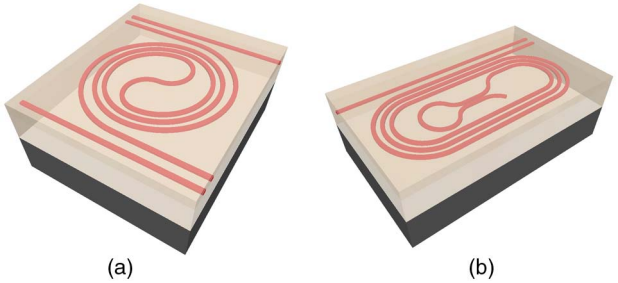

Fig. 2. (a) Schematic representation of a fabricated die featuring the 10 m long Archimedean spiral with a 2 mm minimum bend radius (at the innermost turn-around section). The outermost bend radius was 10 mm. (b) Schematic representation of a fabricated die containing the 0.7 m long spiral delay, with Bézier curves connecting the straight sections. The minimum bend radius of the Bézier curves was 760 μm, while the outermost radius was 1.7 mm. The loop mirror structure can be seen within the spiral center. Both designs in (a) and (b) also feature 21 mm long straight waveguides as auxiliary test structures.

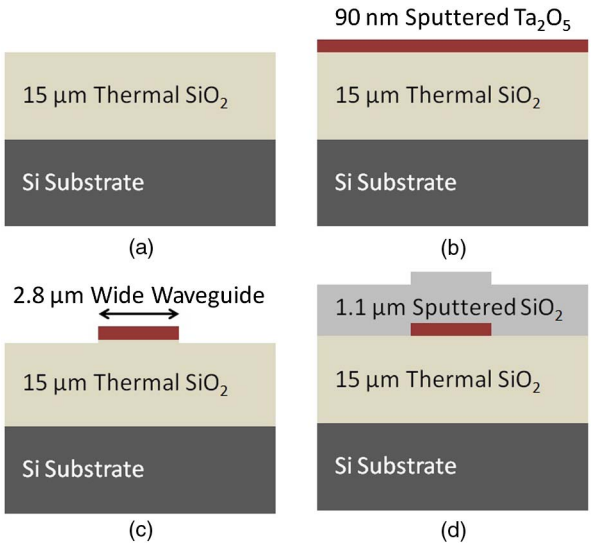

Fig. 3. (a)–(d) Schematic overview of the fabrication process for the waveguides discussed within this paper. All of the processes we employ within this work (including the deposition and etch steps of the Ta_2O_5 material) are CMOS compatible.

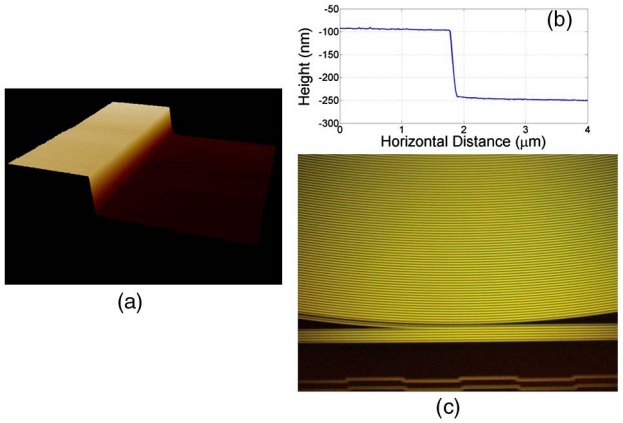

Fig. 4. (a) Three-dimensional AFM image of the $CH_3/CF_4/O_2$ ICP etch of the Ta_2O_5 core. (b) Lateral AFM data quantifying the depth of etch. The deposited core was 90 nm thick but over-etched into the lower thermal SiO_2 cladding for a total etch depth of 150 nm. (c) Dark-field optical micrograph of the bus and outermost waveguides (yellow in color) of the 10 m long Archimedean spiral.

and an optical micrograph of the bus and outermost waveguides of the 10 m long Archimedean spiral. The sidewall roughness of the etching step, a critical factor in achieving low propagation loss, had R_a and R_q (average and RMS) values of 2.4 and 3.0 nm. The measured sidewall angle was 80°. The resulting surface roughness of the deposited Ta_2O_5 core after etching had R_a and R_q values of 0.31 and 0.21 nm. These roughness values, as well as the sidewall angle, are similar to within 10% of what we measure for Si_3N_4-core based waveguides. The patterning and etch steps are followed by a 1.1 μm blanket sputter deposition of the upper SiO_2 cladding. After this last deposition, the 100 mm wafer is diced into separate device die. No facet preparation steps besides dicing were taken before testing the samples.

We first characterized the propagation loss of each die before annealing. This allows for a baseline loss measurement, as well as a

means of assessing the impact of annealing on both the core and cladding materials. Once the initial testing has completed, we anneal the samples in a furnace containing a 3.0 SLPM N_2 flow at 300°C for 3 h. With an Si_3N_4 core material, the nominal anneal temperatures routinely reach 1100°C [12]. This allows for maximum reduction in hydrogen-impurity-related absorption loss [29]. However, the Ta_2O_5 material limits the maximum attainable anneal temperature here, as Ta_2O_5 crystallizes and catastrophically increases in loss. In accordance with the work presented in [26], we determined this point to be temperatures above 650°C. Our final 300°C 3 h annealing protocol was experimentally found to be the optimum temperature/time combination for our sputter-deposited samples. After this final processing step, we then re-characterize the propagation loss.

B. Propagation Loss Characterization by Optical Backscattering Reflectometry

In order to quantify the propagation loss of the Ta_2O_5 waveguides, we utilize the coherent optical frequency domain reflectometry (OFDR) technique using a commercially available system (Luna Inc. OBR 4400) [12,30]. In the OFDR technique, a continuous-wave laser source is scanned over several tens of nm in wavelength (1535–1600 nm in this case), giving a micron-level spatial resolution of the waveguide delay. It is important to note that the OFDR propagation loss measurement is independent of the excess loss and loss uncertainty incurred during fiber-to-chip coupling and is thus more accurate for very low losses than the commonly used cut-back technique. Additionally, over long length spans, OFDR provides optical attenuation versus propagation distance that captures the loss variability caused by localized variations within the fabrication process. This loss variability can be attributed to imperfections, including those due to failed lithography sections of the waveguide core or to flaws such as micron-sized clusters within the nominally homogenous sputter-deposited upper SiO_2 cladding. Figure 5 shows reflection

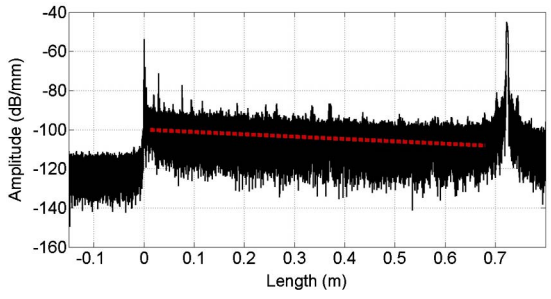

Fig. 5. OBR data from a 0.7 m long spiral delay. The innermost portion of the delay contains a loop mirror reflector, which is clearly visible as a large reflection on the data trace. The other smaller reflection peaks throughout the propagation length are due to scattering events caused by various fabrication imperfections along the waveguide delay. The dashed red line gives a linear fit of the waveguide backscatter averaged over all measured wavelengths. The magnitude of the propagation loss can be approximated as one-half of the slope of this line. Bend loss was not measurable compared to the propagation loss as experienced over the entirety of propagation through the spiral, as evidenced by the constant slope of the measured backscattered power with respect to distance. Utilizing a series of straight waveguides on this same die, we determined through transmission measurements that the fiber-to-chip coupling loss using a cleaved SMF-28 fiber was 3 dB/facet.

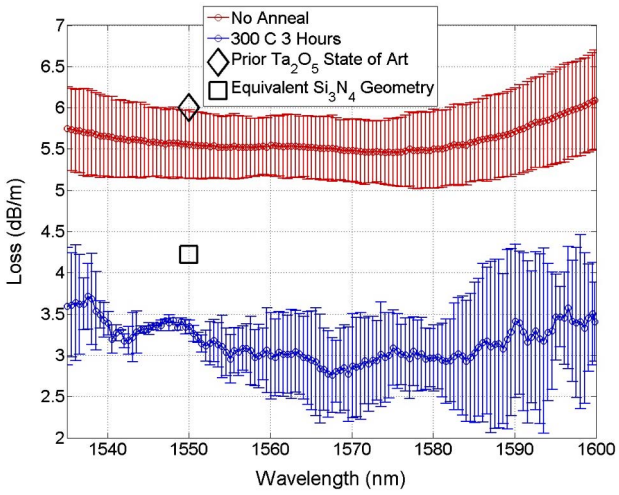

Fig. 6. Propagation loss (mean and standard deviation) versus wavelength for 3 separate die of 10 m long spiral delays. Due to the sputter deposition of the upper cladding, the loss is relatively flat (<2 dB/m spread) over the entirety of the C-band. The prior state of the art Ta_2O_5 measurement result from [25] is shown with a diamond marker. The loss measurement from [27] of an equivalent geometry with a Si_3N_4 core is shown with a square marker.

amplitude data measured for one of the 0.7 m long spiral delays consisting of Bézier curves having minimum bend radii of 760 μm and a central loop mirror structure. Before the OBR scan, the fiber-to-chip coupling and launched polarization are optimized using the OBR source laser, a 3-paddle polarizer, and an infrared camera mounted on a microscope above the sample.

The leftmost peak (near 0 m in distance) is the coupling interface between the fiber and the chip edge. The right peak (near 0.7 m in distance) is the reflection from the on-chip loop mirror structure. It is through this distance relationship that we measured the group index of the waveguide to be 1.55, which agrees with our optical mode simulations and is roughly comparable to that as measured in an Si_3N_4 core waveguide of a similar geometry [27]. Figure 6 shows the mean and standard deviation of the spectral dependence of the propagation loss within 3 separate die of 10 m long Archimedean spirals. As is shown, even the un-annealed samples display a lower loss across the C-band than the previously recorded lowest-loss Ta_2O_5-core waveguide designs [25]. After annealing, the loss is even further reduced to lower than that demonstrated by an Si_3N_4 core waveguide of an equivalent geometry [27]. Due to various scattering events caused by the imperfect nature of the sputtered upper cladding above the entirety of the 10 m spiral, the annealed samples display an irregular standard deviation over the whole of the wavelength range. Such a yield issue is a remaining challenge of fabricating extremely long, ultra-low-loss waveguides.

4. CONCLUSIONS

In conclusion, we have demonstrated record low measured propagation losses for Ta_2O_5-core/SiO_2-clad planar waveguides across the full telecommunications C-band. Our design achieves lower loss than any other reported Ta_2O_5-core waveguide to the best of our knowledge and also simultaneously lower loss than that demonstrated by an Si_3N_4-core waveguide of an equivalent geometry. Our fabrication method, which leverages sputter

deposition of the Ta_2O_5 core and SiO_2 cladding, greatly reduces the incorporation of deleterious hydrogen during the waveguide construction. This approach can be extended to waveguides with even thinner cores, further lowering the expected absolute propagation loss values through a reduction of sidewall scattering loss. Because Ta_2O_5 does not exhibit the material absorption of Si_3N_4 in the C-band, these waveguides could be used for low-loss, high confinement factor designs. Low sidewall scattering loss could be maintained by shallowly etching the core. An initial design for such a low-loss high confinement geometry could consist of a 1.0 μm thick Ta_2O_5 core layer, surrounded by a SiO_2 cladding. Lateral confinement would be accomplished through a 90 nm shallow etch of a 2.8 μm wide waveguide. Such an approach can furthermore facilitate the combination of deeply etched, small bend radius waveguides and shallowly etched ultra-low-loss waveguides on a single chip. Additionally, due to its CMOS compatibility, Ta_2O_5 can readily be used as a replacement for Si_3N_4 in current delay-based applications (gyroscopes, true-time delays, and dispersion compensating filters). Finally, with its favorable nonlinear characteristics, a Ta_2O_5 core waveguide opens up new avenues for device and PIC development, such as in components that leverage nonlinear optics.

Funding. Defense Advanced Research Projects Agency (DARPA) (EPHI HR0011-12-C-0006, iWOG HR0011-14-C-0111); Cisco Systems.

Acknowledgment. The views and conclusions contained in this document are those of the authors and should not be interpreted as representing official policies of the Defense Advanced Research Projects Agency or the U.S. Government.

†These authors contributed equally to this work.

REFERENCES

1. M. Belt and D. J. Blumenthal, "Erbium-doped waveguide DBR and DFB laser arrays integrated within an ultra-low-loss Si_3N_4 platform," Opt. Express **22**, 10655–10660 (2014).
2. D. T. Spencer, J. F. Bauters, M. J. R. Heck, and J. E. Bowers, "Integrated waveguide coupled Si_3N_4resonators in the ultrahigh-Q regime," Optica **1**, 153–157 (2014).
3. M. Belt, J. Bovington, R. Moreira, J. Bauters, M. Heck, J. Barton, J. Bowers, and D. J. Blumenthal, "Sidewall gratings in ultra-low-loss Si_3N_4 planar waveguides," Opt. Express **21**, 1181–1188 (2013).
4. D. Dai, Z. Wang, J. F. Bauters, M.-C. Tien, M. J. R. Heck, D. J. Blumenthal, and J. E. Bowers, "Low-loss Si_3N_4arrayed-waveguide grating (de)multiplexer using nano-core optical waveguides," Opt. Express **19**, 14130–14136 (2011).
5. L. Zhuang, D. Marpaung, M. Burla, W. Beeker, A. Leinse, and C. Roeloffzen, "Low-loss, high-index-contrast Si_3N_4/SiO_2 optical waveguides for optical delay lines in microwave photonics signal processing," Opt. Express **19**, 23162–23170 (2011).
6. M. Burla, D. Marpaung, L. Zhuang, C. Roeloffzen, M. Rezaul Khan, A. Leinse, M. Hoekman, and R. Heideman, "On-chip CMOS compatible reconfigurable optical delay line with separate carrier tuning for microwave photonic signal processing," Opt. Express **19**, 21475–21484 (2011).
7. R. Moreira, J. Garcia, W. Li, J. Bauters, J. S. Barton, M. J. R. Heck, J. E. Bowers, and D. J. Blumenthal, "Integrated ultra-low-loss 4-bit tunable delay for broadband phased array antenna applications," IEEE Photon. Technol. Lett. **25**, 1165–1168 (2013).
8. S. Gundavarapu, T. Huffman, M. Belt, R. Moreira, J. Bowers, and D. Blumenthal, "Integrated ultra-low-loss silicon nitride waveguide coil for optical gyroscopes," in *Optical Fiber Communication Conference*, OSA Technical Digest (Optical Society of America, 2016), paper W4E.5.
9. R. Moreira, S. Gundavarapu, and D. J. Blumenthal, "Programmable eye-opener lattice filter for multi-channel dispersion compensation using an integrated compact low-loss silicon nitride platform," Opt. Express **24**, 16732–16742 (2016).
10. D. J. Moss, R. Morandotti, A. L. Gaeta, and M. Lipson, "New CMOS-compatible platforms based on silicon nitride and Hydex for nonlinear optics," Nat. Photonics **7**, 597–607 (2013).
11. J. S. Levy, A. Gondarenko, M. A. Foster, A. C. Turner-Foster, A. L. Gaeta, and M. Lipson, "CMOS-compatible multiple-wavelength oscillator for on-chip optical interconnects," Nat. Photonics **4**, 37–40 (2010).
12. J. F. Bauters, M. J. R. Heck, D. D. John, J. S. Barton, C. M. Bruinink, A. Leinse, R. G. Heideman, D. J. Blumenthal, and J. E. Bowers, "Planar waveguides with less than 0.1 dB/m propagation loss fabricated with wafer bonding," Opt. Express **19**, 24090–24101 (2011).
13. S. Ezhilvalava and T. Y. Tseng, "Preparation and properties of tantalum pentoxide (Ta_2O_5) thin films for ultra large scale integrated circuits (ULSIs) application—A review," J. Mater. Sci. **10**, 9–31 (1999).
14. C. Chaneliere, J. L. Autran, R. A. B. Devine, and B. Ballard, "Tantalum pentoxide (Ta_2O_5) thin films for advanced dielectric applications," Mater. Sci. Eng. **22**, 269–322 (1998).
15. C.-Y. Tai, J. S. Wilkinson, N. M. B. Perney, M. Caterina Netti, F. Cattaneo, C. E. Finlayson, and J. J. Baumberg, "Determination of nonlinear refractive index in a Ta_2O_5 rib waveguide using self-phase modulation," Opt. Express **12**, 5110–5116 (2004).
16. K. Ikeda, R. E. Saperstein, N. Alic, and Y. Fainman, "Thermal and Kerr nonlinear properties of plasma-deposited silicon nitride/silicon dioxide waveguides," Opt. Express **16**, 12987–12994 (2008).
17. J. Robertson, "Band offsets of wide-band-gap oxides and implications for future electronic devices," J. Vac. Sci. Technol. B **18**, 1785–1791 (2000).
18. C.-L. Wu, C.-H. Hsieh, G.-R. Lin, W.-C. Chi, Y.-J. Chiu, Y.-Y. Lin, Y.-J. Hung, M.-H. Shih, A.-K. Chu, and C.-K. Lee, "Tens of GHz Tantalum pentoxide-based micro-ring all-optical modulator for Si photonics," Ann. Phys. **529**, 1600358 (2016).
19. C. Lacava, A. Aghajani, P. Hua, D. J. Richardson, P. Petropoulos, and J. Wilkinson, "Nonlinear optical properties of ytterbium-doped tantalum pentoxide rib waveguides on silicon at telecom wavelengths," in *Optical Fiber Communication Conference*, OSA Technical Digest (Optical Society of America, 2016), paper W4E.4.
20. A. Subramanian, "Tantalum pentoxide waveguide amplifier and laser for planar lightwave circuits," Ph.D. dissertation (University of Southampton, 2011).
21. C. Christensen, R. de Reus, and S. Bouwstra, "Tantalum oxide thin films as protective coatings for sensors," J. Micromech. Microeng. **9**, 113–118 (1999).
22. A. Aghajani, G. S. Murugan, N. P. Sessions, V. Apostolopoulos, and J. S. Wilkinson, "Waveguide lasers in ytterbium-doped tantalum pentoxide on silicon," Opt. Lett. **40**, 2549–2552 (2015).
23. A. Z. Subramanian, C. J. Oton, D. P. Shepherd, and J. S. Wilkinson, "Erbium doped waveguide laser in tantalum pentoxide," IEEE Photon. Technol. Lett. **22**, 1571–1573 (2010).
24. C.-L. Wu, B.-T. Chen, Y.-Y. Lin, W.-C. Tien, G.-R. Lin, Y.-J. Chiu, Y.-J. Hung, A.-K. Chu, and C.-K. Lee, "Low-loss and high-Q Ta2O5 based micro-ring resonator with inverse taper structure," Opt. Express **23**, 26268–26275 (2015).
25. M. Itoh, T. Kominato, M. Abe, M. Itoh, and T. Hashimoto, "Low-loss silica-based SiO_2-Ta_2O_5 Waveguides With extremely high δ fabricated using sputtered thin films," J. Lightwave Technol. **33**, 318–323 (2015).
26. M. Zhu, Z. Zhang, and W. Miao, "Intense photoluminescence from amorphous tantalum oxide films," Appl. Phys. Lett. **89**, 021915 (2006).
27. J. F. Bauters, M. J. R. Heck, D. John, D. Dai, M.-C. Tien, J. S. Barton, A. Leinse, R. G. Heideman, D. J. Blumenthal, and J. E. Bowers, "Ultra-low-loss high-aspect-ratio Si_3N_4 waveguides," Opt. Express **19**, 3163–3174 (2011).
28. J. F. Bauters, M. L. Davenport, M. J. R. Heck, J. K. Doylend, A. Chen, A. W. Fang, and J. E. Bowers, "Silicon on ultra-low-loss waveguide photonic integration platform," Opt. Express **21**, 544–555 (2013).
29. F. Ay and A. Aydinli, "Comparative investigation of hydrogen bonding in silicon based PECVD grown dielectrics for optical waveguides," Opt. Mater. **26**, 33–46 (2004).
30. B. J. Soller, D. K. Gifford, M. S. Wolfe, and M. E. Froggatt, "High resolution optical frequency domain reflectometry for characterization of components and assemblies," Opt. Express **13**, 666–674 (2005).